Estimation of Time-Varying Origin–Destination Patterns for Design of Multipath Progression on a Signalized Arterial

Xianfeng Yang and Gang-Len Chang

Most state-of-the-art control strategies for coping with arterial congestion provide progression for heavy through-traffic flows. However, such strategies cannot tackle arterial congestion caused by both heavy turning and through-traffic flows, where turning-traffic volumes often spill over their designated bay length and cause link blockage. An effective approach is to offer a progression band to each of those critical path flows that can be identified from the arterial origin–destination (O-D) flow patterns. This study proposes three models for estimating such information from available traffic measurements. The estimated time-varying O-D distributions yield both the number of critical path flows and their respective volume ranks for design of their progression bands. Based on the principle of flow conservations, the first model captures the relationships between link counts and dynamic O-D flows, whereas the second model directly takes turning flows at each intersection as the primary model input. To consider further the impact of traffic signal plans on O-D flow patterns, the third model incorporates a set of additional measurements—the time-varying queue length information—to improve the estimation accuracy. Comparisons of the actual O-D flows and the estimated results demonstrate the effectiveness of the proposed models for identifying the heavy flow paths and their respective volumes.

Providing two-way signal progression for congested arterials has long been viewed by traffic professionals as one of the most effective control strategies. However, depending on the distribution of flow patterns, the signal plan designed to favor through traffic may cause unexpected traffic queue spillback at intersections that need to accommodate heavy turning volumes. For instance, serving mainly as connectors between a freeway corridor and a neighboring urban network, some arterials' predominant traffic flows may not be for through movements only but are likely to combine both turning and through movements. To progress all traffic movements on such congested arterials experiencing multiple heavy path flows, Yang et al. proposed a multipath signal progression model to facilitate not only the through traffic but all identified critical path flows (*1*). The most critical information for design of such an effective multipath progression is the time-varying distribution of the arterial's O-D flows.

A review of the related literature shows that few studies on estimating O-D patterns for signalized arterials. Of those, Lou and Yin used detected link counts to develop a decomposition framework for estimating time-varying dynamic O-D flows on an arterial (*2*). Their proposed framework is to first decompose the entire arterial into a set of individual intersections and then to perform the estimation of turning flows with link counts, which in turn serve as the measurements for the arterial O-D estimation. That pioneering work, however, did not address the impact of implemented signal plans on observable time-varying link flows and consequently on the estimation accuracy of the resulting O-D patterns. For estimating time-dependent turning fractions at intersections, Chang and Tao incorporated additional constraints from signal timing information in their enhanced model. The results of extensive simulation experiments indicate that such methods can yield more accurate estimation, compared with the base model, without considering the impact of signal timings (*3*).

Despite the scanty literature on arterial O-D estimation, there is a large body of models for estimating O-D demands on general networks (*4–6*), and most of these fall into either of the two main categories: assignment-based (*7–9*) and nonassignment-based (*10–13*) models. The former category of studies is grounded in the prerequisite that a reliable prior time-varying O-D set and a dynamic traffic assignment model are available for model construction and estimation. To circumvent the prerequisite, some researchers have proposed nonassignment-based models, intending to use only the time series of available link volume counts for estimation, reducing the dependency of a dynamic traffic assignment model. However, none of these studies addressed the critical impacts of signal presence and different timing plans on the time-varying distributions of network O-D flows. Aside from these two categories of studies, some researchers have taken advantage of additional information, measured from emerging sensing technologies, to increase the developed model's observability. Examples of studies along this line are the use of automatic vehicle identification systems (*14*), vehicle plate scanning (*15*), sporadic routing data (*16*), GPS probe vehicles (*17*), and cell phone data (*18*).

This study followed the research line of nonassignment-based methods and estimated the time-varying O-D matrix on a signalized arterial. Depending on information availability in practice, this study proposed three models for capturing the relationships between

X. Yang, Department of Civil, Construction, and Environmental Engineering, College of Engineering, San Diego State University, 5500 Campanile Drive, San Diego, CA 92182. G.-L. Chang, Department of Civil and Environmental Engineering, A. James Clark School of Engineering, University of Maryland, College Park, 1173 Glenn Martin Hall, College Park, MD 20742. Corresponding author: X. Yang, xyang@mail.sdsu.edu

Transportation Research Record: Journal of the Transportation Research Board, No. 2667, 2017, pp. 28–38.
http://dx.doi.org/10.3141/2667-04

time-varying O-D flows and the observable measurements. Following the same notation of studies on estimating intersection turning ratios (*19, 20*), Model 1 extends the method to use link flows for arterial time-varying O-D estimation. To improve the estimation accuracy, other studies also used the turning movement counts as model input (*6*). Similarly, this study's proposed Model 2 took the turning flows at each intersection as the primary model input. Because of the emergence of queue detectors for intersection signal control, this study further took the measurable queue information in the Model 3 formulations because the evolution of time-varying queue patterns offers valuable information reflecting the interrelationships between the observable arterial's O-D flows and its signal plans. More specifically, under the same level of traffic demand, the queue length at a given link is expected to be relatively short if most of its arriving flows are coordinated with neighboring traffic signals. Hence, by constructing the interrelationships between traffic counts from detectors, the signal plan, and the observed queue length evolution, one can better estimate the origin of arriving flows (e.g., the turning traffic from side streets or through flows from upstream intersections) and their destinations with proper algorithms.

MODEL DEVELOPMENT

To estimate the time-varying O-D flow pattern on the signalized arterial, this study developed three models based on data availability. Model 1 uses link counts as input, Model 2 takes the measurement of intersection turning flows, and Model 3 extends Model 2 by further using real-time queue length information.

Model 1 Formulations

Considering a signalized arterial of N intersections as shown in Figure 1, Model 1 takes its link counts as the primary input for its O-D estimation. All detectors are assumed to be placed at the upstream location of each link.

With the available link counts data during each time interval k, the information ready for use includes the time series of entering flows $q_i(k)$, leaving flows $y_i(k)$, and link flows $u_l^{\text{in}}(k)$ and $u_l^{\text{out}}(k)$. Then one can construct the following relationships, based on the flow conservations at each intersection, as shown in Figure 1:

$$q_i(k) = \sum_{j=1}^{2N+2} f_{ij}(k) \tag{1}$$

$$f_{ij}(k) = q_i(k) b_{ij}(k) \tag{2}$$

where $f_{ij}(k)$ is the number of vehicles entering the arterial from origin node i to destination node j during time interval k, and $b_{ij}(k)$ denotes the fraction of flow $q_i(k)$, which has the destination of node j.

Because of speed variations among drivers, those concurrently entering node i may take a different number of time intervals to arrive at node j. Assuming that the travel times of those drivers are distributed among multiple consecutive time intervals, one can then formulate the exiting traffic volumes as follows:

$$y_j(k) = \sum_{m=0}^{M} \sum_{i=1}^{2N+2} q_i(k-m) \rho_{ij}^m(k-m) b_{ij}(k-m) \tag{3}$$

$$\sum_{m=0}^{M} \rho_{ij}^m(k-m) = 1 \tag{4}$$

where $\rho_{ij}^m(k)$ is the fraction of $f_{ij}(k)$ vehicles that takes m time intervals to reach a detector at node j during time interval k, and M is the maximum number of intervals for a vehicle to travel from origin to destination.

Also note that the flow measurements between neighboring intersections, $u_i(k)$, can provide additional valuable information to construct the following equations:

$$u_l^{\text{in}}(k) = \sum_{m=0}^{M} \sum_{i=1}^{2l+1} \sum_{j=2l+2}^{2N+2} q_i(k-m) \theta_l^m(k-m) b_{ij}(k-m) \tag{5}$$

$$u_l^{\text{out}}(k) = \sum_{m=0}^{M} \sum_{i=2l}^{2N+2} \sum_{j=1}^{2l-1} q_i(k-m) \theta_{il}^m(k-m) b_{ij}(k-m) \tag{6}$$

where $\theta_{il}^m(k)$ denotes a fraction of $f_{ij}(k)$ vehicles that take m time intervals to arrive at intersection l during time interval k. Equations 1 through 6 can be implemented to capture the dynamic relationships between the O-D patterns and link flows.

However, the above system formulations contain many state variables, that is, $b_{ij}(k)$, $\rho_{ij}^m(k)$, and $\theta_{il}^m(k)$. The number of these unknown parameters increases with the required M value (i.e., the maximum time intervals). As such, more information and refinement steps are necessary to ensure the computing efficiency and tractability of this proposed model.

To deal with the many unknown parameters, Chang and Wu simplified the formulations by assuming that the speeds of vehicles

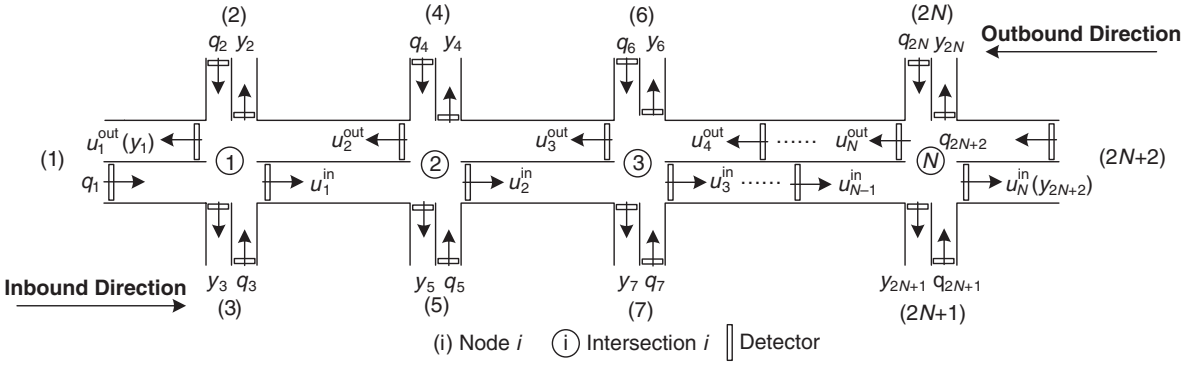

FIGURE 1 Typical local arterial segment.

entering the network at the same time interval are likely to be distributed in a small range (*11*). Following the same logic, this study assumed that the variation of vehicle travel times between nodes *i* and *j* is within an interval, $[\tau_{ij}^{k-}, \tau_{ij}^{k+}]$. In practice, the travel time would be time-dependent and be varied with different congestion levels. Hence, estimation of link travel time is required before the model is implemented. Denoting $\mu_{ij}(k)$ as the average travel time from node *i* to node *j* during time interval *k*, Equations 3 to 6 can be rewritten as follows:

$$y_j(k) = \sum_{i=1}^{2N+2} \begin{bmatrix} q_i\left(k-\tau_{ij}^{k+}\right)\rho_{ij}^{+}\left(k-\tau_{ij}^{k+}\right)b_{ij}\left(k-\tau_{ij}^{k+}\right) \\ +\, q_i\left(k-\tau_{ij}^{k-}\right)\rho_{ij}^{-}\left(k-\tau_{ij}^{k-}\right)b_{ij}\left(k-\tau_{ij}^{k-}\right) \end{bmatrix} \tag{7}$$

$$\rho_{ij}^{+}(k) + \rho_{ij}^{-}(k) = 1 \tag{8}$$

$$u_l^{\text{in}}(k) = \sum_{i=1}^{2l+1}\sum_{j=2l+2}^{2N+2} \begin{bmatrix} q_i\left(k-\tau_{il}^{k+}\right)\theta_{il}^{+}\left(k-\tau_{il}^{k+}\right)b_{ij}\left(k-\tau_{il}^{k+}\right) \\ +\, q_i\left(k-\tau_{il}^{k-}\right)\theta_{il}^{-}\left(k-\tau_{il}^{k-}\right)b_{ij}\left(k-\tau_{il}^{k-}\right) \end{bmatrix} \tag{9}$$

$$u_l^{\text{out}}(k) = \sum_{i=2l}^{2N+2}\sum_{j=0}^{2l-1} \begin{bmatrix} q_i\left(k-\tau_{il}^{k-}\right)\theta_{il}^{-}\left(k-\tau_{il}^{k-}\right)b_{ij}\left(k-\tau_{il}^{k-}\right) \\ +\, q_i\left(k-\tau_{il}^{k-}\right)\theta_{il}^{-}\left(k-\tau_{il}^{k-}\right)b_{ij}\left(k-\tau_{il}^{k-}\right) \end{bmatrix} \tag{10}$$

$$\theta_{il}^{+}(k) + \theta_{il}^{-}(k) = 1 \tag{11}$$

where

$$\tau_{ij}^{k-} = \text{int}\left[\frac{\mu_{ij}(k)}{\Delta t}\right] \text{and } \tau_{ij}^{k+} = \tau_{ij}^{k-} + 1$$

$$\rho_{ij}^{+}(k) = \rho_{ij}^{\tau_{ij}^{k+}}(k) \text{ and } \rho_{ij}^{-}(k) = \rho_{ij}^{\tau_{ij}^{k-}}(k)$$

$$\theta_{ij}^{+}(k) = \theta_{ij}^{\tau_{ij}^{k+}}(k) \text{ and } \rho_{ij}^{-}(k) = \rho_{ij}^{\tau_{ij}^{k-}}(k)$$

Model 2 Formulations

Because of the indeterminate nature of the O-D estimation system, increasing the number of observable measurements can greatly enhance estimation accuracy. Lou and Yin derived a decomposition model to estimate O-D flows on signalized arterials, where the turning flows—estimated at the first stage—serve as the measurement for estimation at the second stage (*2*). However, the potential estimation errors from Stage 1 estimation are likely to propagate to State 2 computations. Since the technology for detecting intersection turning flows is available in practice, Model 2 focuses on modeling the interrelationships between the O-D patterns and intersection turning flows.

For convenience of discussion, this study redefined the notation for turning flows at each intersection. As shown in Figure 2, η_{il}^{L}, η_{il}^{T}, and η_{il}^{R} denote the flows of left-turn, through, and right-turn movements for leg *i* at intersection *l*.

Then, one can construct the following relationships between the O-D flows and the turning flows for Approaches 1 and 3 of intersection *l* with the notation shown in Figure 2:

$$\eta_{1,l}^{L}(k) = \sum_{m=\tau_{2l,l}^{-}}^{\tau_{2l,l}^{-}+1}\sum_{j=2l+2}^{2N+2} q_{2l}(k-m)\theta_{2l,l}^{m}(k-m)b_{2l,j}(k-m) \tag{12}$$

$$\eta_{1,l}^{T}(k) = \sum_{m=\tau_{2l,l}^{-}}^{\tau_{2l,l}^{-}+1} q_{2l}(k-m)\theta_{2l,l}^{m}(k-m)b_{2l,2l+1}(k-m) \tag{13}$$

$$\eta_{1,l}^{R}(k) = \sum_{m=\tau_{2l,l}^{-}}^{\tau_{2l,l}^{-}+1}\sum_{j=1}^{2l-1} q_{2l}(k-m)\theta_{2l,l}^{m}(k-m)b_{2l,j}(k-m) \tag{14}$$

$$\eta_{3,l}^{L}(k) = \sum_{m=\tau_{2l+1,l}^{-}}^{\tau_{2l+1,l}^{-}+1}\sum_{j=1}^{2l-1} q_{2l+1}(k-m)\theta_{2l+1,l}^{m}(k-m)b_{2l+1,j}(k-m) \tag{15}$$

$$\eta_{3,l}^{T}(k) = \sum_{m=\tau_{2l+1,l}^{-}}^{\tau_{2l+1,l}^{-}+1} q_{2l+1}(k-m)\theta_{2l+1,l}^{m}(k-m)b_{2l+1,2l}(k-m) \tag{16}$$

$$\eta_{3,l}^{R}(k) = \sum_{m=\tau_{2l+1,l}^{-}}^{\tau_{2l+1,l}^{-}+1}\sum_{j=2l+2}^{2N+2} q_{2l+1}(k-m)\theta_{2l+1,l}^{m}(k-m)b_{2l+1,j}(k-m) \tag{17}$$

As well, one can construct the relationships between the O-D flows and the turning flows for Approaches 2 and 4 of intersection *l* with the following equations:

$$\eta_{2l}^{L}(k) = \sum_{m=\tau_{il}^{-}}^{\tau_{il}^{-}+1}\sum_{i=2l+2}^{2N+2} q_i(k-m)\theta_{i,l}^{m}(k-m)b_{i,2l+1}(k-m) \tag{18}$$

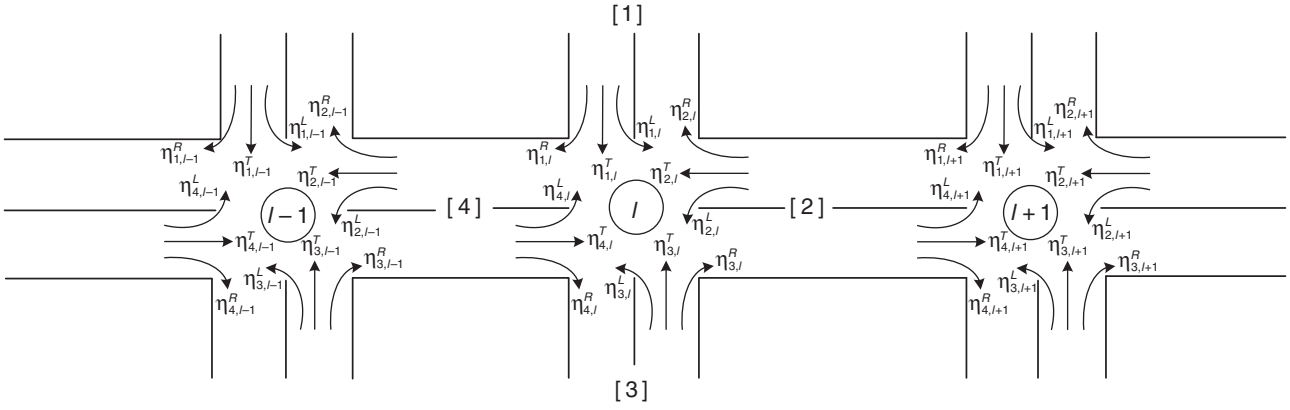

FIGURE 2 Notation used in Model 2 for intersection *l* and turning flows.

$$\eta_{2l}^{T}(k)=\sum_{m=\tau_{il}^{-}+1}^{\tau_{il}^{+}+1}\sum_{i=2l+2}^{2N+2}\sum_{j=1}^{2l-1}q_i(k-m)\theta_{i,l}^{m}(k-m)b_{ij}(k-m) \tag{19}$$

$$\eta_{2l}^{R}(k)=\sum_{m=\tau_{il}^{-}+1}^{\tau_{il}^{+}+1}\sum_{i=2l+2}^{2N+2}q_i(k-m)\theta_{i,l}^{m}(k-m)b_{i,2l}(k-m) \tag{20}$$

$$\eta_{4l}^{L}(k)=\sum_{m=\tau_{il}^{-}+1}^{\tau_{il}^{+}+1}\sum_{i=1}^{2l-1}q_i(k-m)\theta_{i,l}^{m}(k-m)b_{i,2l}(k-m) \tag{21}$$

$$\eta_{4l}^{T}(k)=\sum_{m=\tau_{il}^{-}+1}^{\tau_{il}^{+}+1}\sum_{i=1}^{2l-1}\sum_{j=2l+2}^{2N+2}q_i(k-m)\theta_{i,l}^{m}(k-m)b_{ij}(k-m) \tag{22}$$

$$\eta_{4l}^{R}(k)=\sum_{m=\tau_{il}^{-}+1}^{\tau_{il}^{+}+1}\sum_{i=1}^{2l-1}q_i(k-m)\theta_{i,l}^{m}(k-m)b_{i,2l+1}(k-m) \tag{23}$$

Model 3 Formulations

The number of measurements in both Model 1 and Model 2 is always less than the number of parameters to be estimated [$(2N+2)(5N+4)$]. Hence, creatively identifying additional observable relationships to augment the system's observability is essential to increase the accuracy of such dynamic O-D estimation models. A new set of system relationships proposed in Model 3 is to formulate the interrelationships between the observable intersection and the arterial signal plans, which may vary with the time-varying O-D distributions.

Figure 3 shows a typical arterial segment, consisting of two adjacent intersections. The target link, connecting these two intersections, has three source flows: $\eta_{1,l}^{R}$, $\eta_{2,l}^{T}$, and $\eta_{3,l}^{L}$; and three outflows: $\eta_{2,l-1}^{L}$, $\eta_{2,l-1}^{T}$, and $\eta_{2,l-1}^{R}$. To hold the flow conservations using traffic counts, one can reach the following relationships:

$$\eta_{2,l-1}^{L}(k)+\eta_{2,l-1}^{T}(k)+\eta_{2,l-1}^{R}(k)=\eta_{1,l}^{R}(k-m')+\eta_{2,l}^{T}(k-m')+\eta_{3,l}^{L}(k-m') \tag{24}$$

where m' is the travel time from intersection l to intersection $l-1$.

Conceivably, any O-D flow patterns, consistent with Equation 24, could be the same set of feasible solutions yielded by Models 1 and 2. However, if queue detectors have been deployed, the relationships between the queue variation and signals offer another set of constraints with which to improve model estimation; different O-D flow patterns may result in different queue lengths on the connecting links because of the impact of traffic signals. With the through queue in Figure 3 as an example and assuming that the signal progression is provided to the through traffic along the arterial, Figure 4 shows the discrepancy on traffic queue patterns between two scenarios in which the same numbers of vehicles per cycle arrive at the intersection but come from different origins. In practice, video sensors with image processing algorithms and radar sensors with some embedded estimation function satisfy the data collection need in this model.

Figure 4*a* illustrates the queue formation patterns when most queuing vehicles are from the turning source flows, such as $\eta_{1,l}^{R}$ and $\eta_{3,l}^{L}$. In contrast, Figure 4*b* shows the resulting queue patterns when most of those vehicles are from the upstream through flows $\eta_{2,l}^{T}$. Since the progression is for through movements on the arterial traffic, the through flows from intersection l are most likely to encounter a green phase at intersection $l-1$, whereas the turning flows will experience mainly the red phase. Hence, depending on the contributing sources of vehicles that constitute the arriving flow patterns, the resulting queue pattern may differ significantly even with the same number of arrivals. More specific, the time-varying queue patterns at an intersection are highly correlated with the O-D flows and intersection signal timings. As such, one may consider incorporating such additional information in formulating the intersection O-D estimation model.

With the link shown in Figure 3 as an example, the enhanced model formulations, using the additional time-varying queue information, are as follows:

$$\delta_{l,l-1}^{T}(k)=\sigma_{l,l-1}^{T}(k)+\varphi_T\left(\eta_{1,l}^{R}\xi_{1,l}^{T}r_1^{T}+\eta_{2,l}^{T}\xi_{2,l}^{T}r_{2,l}^{T}+\eta_{3,l}^{L}\xi_{3,l}^{T}r_{3,l}^{T}\right) \tag{25}$$

$$\delta_{l,l-1}^{L}(k)=\sigma_{l,l-1}^{L}(k)+\varphi_L\left(\eta_{1,l}^{R}\xi_{1,l}^{L}r_1^{L}+\eta_{2,l}^{T}\xi_{2,l}^{L}r_{2,l}^{L}+\eta_{3,l}^{L}\xi_{3,l}^{L}r_{3,l}^{L}\right) \tag{26}$$

$$\delta_{l,l-1}^{R}(k)=\sigma_{l,l-1}^{R}(k)+\varphi_R\left(\eta_{1,l}^{R}\xi_{1,l}^{R}r_1^{R}+\eta_{2,l}^{T}\xi_{2,l}^{R}r_{2,l}^{R}+\eta_{3,l}^{L}\xi_{3,l}^{R}r_{3,l}^{R}\right) \tag{27}$$

where

$\delta_{l,l-1}^{i}(k)$ = queue length at the end of a red phase on lane group i,
$\sigma_{l,l-1}^{i}(k)$ = queue length at the start of a red phase on lane group i,

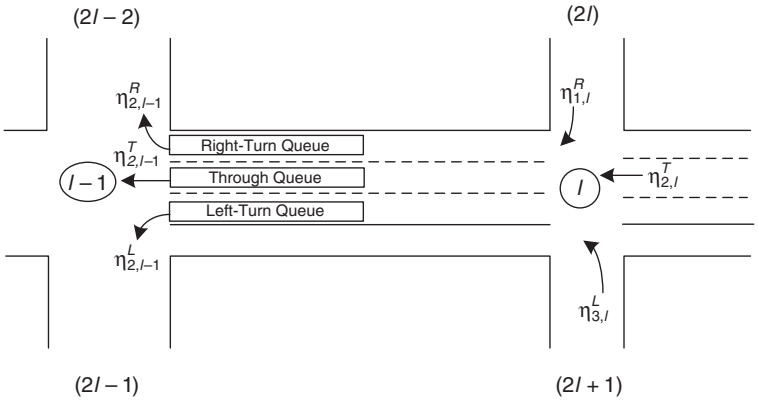

FIGURE 3 Flow diverging and conservation at two adjacent intersections, l and $l-1$.

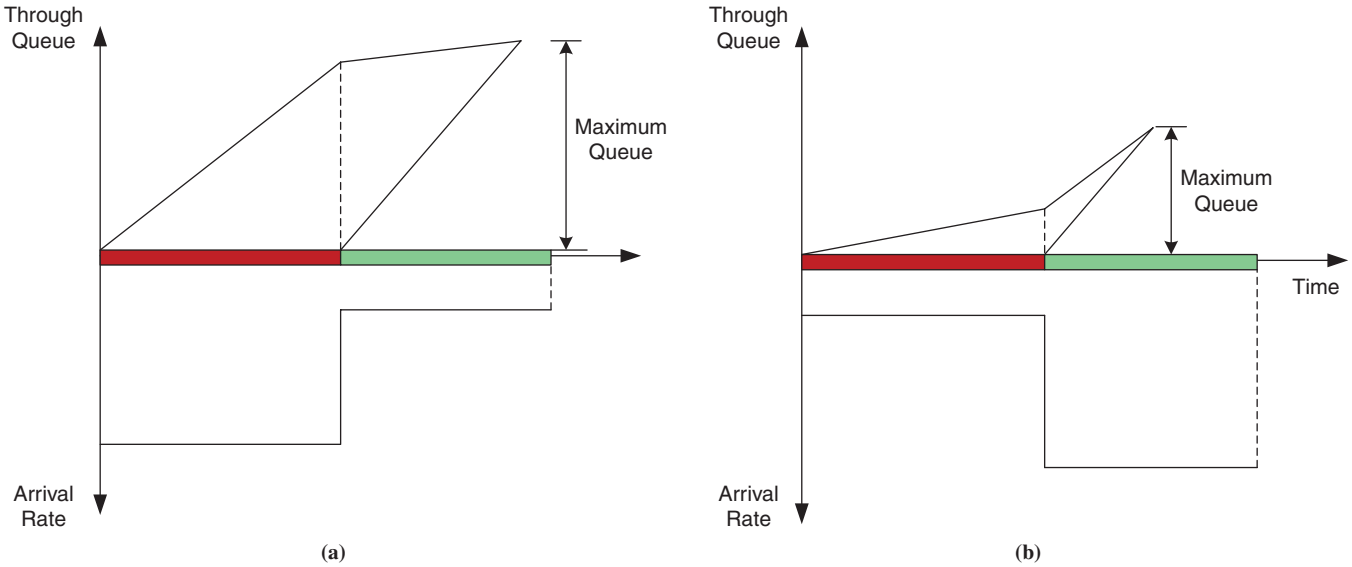

FIGURE 4 Formation of through queue by arrival pattern.

φ_i = lane use factor for lane group i that accounts for the uneven distribution of flows on different lanes, and
$\xi_{i,l}^{j}$ = ratio of flows $\eta_{i,l}^{m}$ that will join the downstream flows $\eta_{2,l-1}^{j}$, where

$$\xi_{i,l}^{L}+\xi_{i,l}^{T}+\xi_{i,l}^{R}=1 \qquad \forall i=1,2,3 \tag{28}$$

$r_{i,l}^{j}$ is the ratio of uncoordinated flows that can be approximated as

$$r_{i,l}^{j}=\frac{\phi_{i,l}^{j}}{\Delta T} \tag{29}$$

and $\phi_{i,l}^{j}$ is the progression duration within one time interval.

For convenience of computation, this study set the common cycle length to equal the length of estimation time interval, letting the value of $r_{i,l}^{j}$ be fixed in a pretimed signal control system.

On the basis of Equations 12 to 23, one can further reformulate Equations 25 to 27 as follows:

$$\delta_{l,l-1}^{p}(k)=\sigma_{l,l-1}^{p}(k)+\varphi_T\left[\begin{array}{l}\left(\sum_{m=\tau_{2,l}^{-}}^{\tau_{2,l}^{-}+1}\sum_{j=1}^{2l-1}q_{2l}(k-m)\theta_{2l,l}^{m}(k-m)b_{2l,j}(k-m)\right)\xi_{1,l}^{p}r_{1}^{p}\\ +\left(\sum_{m=\tau_{il}^{-}}^{\tau_{il}^{-}+1}\sum_{i=2l+2}^{2N+2}\sum_{j=1}^{2l-1}q_{i}(k-m)\theta_{i,l}^{m}(k-m)b_{ij}(k-m)\right)\xi_{2,l}^{p}r_{2,l}^{p}\\ +\left(\sum_{m=\tau_{2l+1,l}^{-}}^{\tau_{2l+1,l}^{-}+1}\sum_{j=1}^{2l-1}q_{2l+1}(k-m)\theta_{2l+1,l}^{m}(k-m)b_{2l+1,j}(k-m)\right)\xi_{3,l}^{p}r_{3,l}^{p}\end{array}\right] \qquad \forall p\in\{L,T,R\} \tag{30}$$

Equation 30 is derived for the outbound flows from intersection l to $l-1$. For the inbound flows from intersection l to $l+1$, one can derive the same relationships between $\delta_{l,l+1}^{i}(k)$ and O-D parameters as follows:

$$\delta_{l,l+1}^{p}(k)=\sigma_{l,l+1}^{p}(k)+\varphi_T\left[\begin{array}{l}\left(\sum_{m=\tau_{2,l}^{-}}^{\tau_{2,l}^{-}+1}\sum_{j=2l+2}^{2N+2}q_{2l}(k-m)\theta_{2l,l}^{m}(k-m)b_{2l,j}(k-m)\right)\xi_{1,l}^{p}r_{1}^{p}\\ +\left(\sum_{m=\tau_{il}^{-}}^{\tau_{il}^{-}+1}\sum_{i=1}^{2l-1}\sum_{j=2l+2}^{2N+2}q_{i}(k-m)\theta_{i,l}^{m}(k-m)b_{ij}(k-m)\right)\xi_{2,l}^{p}r_{2,l}^{p}\\ +\left(\sum_{m=\tau_{2l+1,l}^{-}}^{\tau_{2l+1,l}^{-}+1}\sum_{j=2l+2}^{2N+2}q_{2l+1}(k-m)\theta_{2l+1,l}^{m}(k-m)b_{2l+1,j}(k-m)\right)\xi_{3,l}^{p}r_{3,l}^{p}\end{array}\right] \qquad \forall p\in\{L,T,R\} \tag{31}$$

ESTIMATION ALGORITHM

As used in most existing approaches, the dynamic O-D parameters $b_{ij}(k)$, $\rho_{ij}^{-}(k)$, and $\theta_{il}^{-}(k)$ are assumed to follow the random walk process between successive time intervals, as shown in the following equations:

$$b_{ij}(k+1)=b_{ij}(k)+w_{ij}^{b}(k) \qquad 1\le i;\ j\le 2N+2 \tag{32}$$

$$\rho_{ij}^{-}(k+1)=\rho_{ij}^{-}(k)+w_{ij}^{\rho}(k) \qquad 1\le i;\ j\le 2N+2 \tag{33}$$

$$\theta_{il}^{-}(k+1)=\theta_{il}^{-}(k)+w_{il}^{\theta}(k) \qquad 1\le i\le 2N+2;\ 1\le l\le N \tag{34}$$

where the random terms $w_{ij}^{b}(k)$, $w_{ij}^{\rho}(k)$, and $w_{il}^{\theta}(k)$ are independent Gaussian white noise with zero means. These error terms of O-D parameters do not typically follow a Gaussian distribution because a Gaussian distribution extends infinitely in both directions. However,

one can use a transformation to convert the non-Gaussian data to a Gaussian distribution.

To facilitate the presentation, define the parameters of Model 1 as follows:

$$\mathbf{X}(k)=\begin{bmatrix}\mathbf{B}(k)\\ \mathbf{P}(k)\\ \mathbf{\Theta}(k)\end{bmatrix} \tag{35}$$

$$\mathbf{W}(k)=\begin{bmatrix}\mathbf{W}^{\mathbf{b}}(k)\\ \mathbf{W}^{\mathbf{\rho}}(k)\\ \mathbf{W}^{\mathbf{\theta}}(k)\end{bmatrix} \tag{36}$$

where

$$\mathbf{B}(k)=\left[b_{ij}(k)\right]_{(2N+2)^2\times 1}$$

$$\mathbf{P}(k)=\left[\rho_{ij}^{-}(k)\right]_{(2N+2)^2\times 1}$$

$$\mathbf{\Theta}(k)=\left[\theta_{il}(k)\right]_{N(2N+2)\times 1}$$

and

$\mathbf{W}^{\mathbf{b}}(k)$, $\mathbf{W}^{\mathbf{\rho}}(k)$, and $\mathbf{W}^{\mathbf{\theta}}(k)$ = matrices of error terms.

Hence, one can obtain the matrix form of Equations 12 to 14 as follows:

$$\mathbf{X}(k+1)=\mathbf{X}(k)+\mathbf{W}(k) \tag{37}$$

With the above transformation for $\mathbf{B}(k)$, the observation system in Equations 8 to 12 can be restructured into the following matrix form:

$$\mathbf{Z}(k+1)=\mathbf{H}(k)\cdot\mathbf{X}(k)+\mathbf{e}(k) \tag{38}$$

where $\mathbf{Z}(k) = [q_1(k), q_2(k), \ldots, q_{2N+2}(k), y_1(k), y_2(k), \ldots, y_{2N+2}(k), u_2(k), u_3(k), \ldots, u_{2N-1}(k)]^T$. In the equation, $\mathbf{Z}(k)$ is a column vector of dimension $2(2N + 2) + (2N - 2)$, and $\mathbf{e}(k)$ is an observation noise vector of the same dimension, which can be taken as Gaussian white noises with zero mean and covariance matrix $\mathbf{R}$.

Denote $h(.)$ as the measurement functions, shown by Equations 1, 7, 9, and 10; then $\mathbf{H}(x)$ is the Jacobian matrix of partial derivatives of the function, $h(.)$, with respect to the estimation state x:

$$\mathbf{H}_{[rs]}(k)=H_{rs}^{k}=\frac{\partial h_{[r]}(\mathbf{X}(k))}{\partial \mathbf{X}_{[s]}} \tag{39}$$

So far, a canonical state–space system model, Equations 36 to 40, has been established. Because of the nonlinear nature of the formulations and for computing efficiency, this study used the extended Kalman filter algorithm to perform the sequential estimation. A step-by-step illustration of the estimation algorithm is presented in Equation Box 1. A similar solution algorithm can be applied to Models 2 and 3.

EQUATION BOX 1 Estimation Algorithm Using Extended Kalman Filter

Step 0. Initialize.

- Set the length of time interval Δt.
- Initialize the parameters $b_{ij}(0)$, $\rho_{ij}^{-}(0)$, and $\theta_{il}^{-}(0)$.

Step 1. Compute the mean travel time as follows:

$$\mu_{ij}(k)=\frac{L_{ij}}{v_{ij}(k)}+\sum_{l\in\delta_{ij}}d_l(k)$$

where L_{ij} is the travel distance between node i and j; $v_{ij}(k)$ is the average travel speed; δ_{ij} is the set of intersections included in the path i to j; and $d_l(k)$ is the average delay at intersection l, which can be estimated with existing models, such as that in the *Highway Capacity Manual* (*21*).

Step 2. Compute the linearized transformation matrix $\mathbf{H}(k)$.

$$\text{e.g., } \frac{\partial q_i(k)}{\partial b_{ij}(k)}=q_i(k);\ \frac{\partial u_l^{\text{out}}(k)}{\partial b_{ij}(k)}=q_i(k)\theta_{i,l}^{-}(k)\qquad i\geq l+1;\ j\leq l$$

Step 3. Initialize the extended Kalman filtering.

- Set $\mathbf{X}(0)=[\mathbf{B}(0)\,\mathbf{P}(0)\,\mathbf{\Theta}(0)]$;
- Set $\mathbf{P}^{-}(0)$ and Q; where $\mathbf{P}^{-}(k)$ is the covariance matrix of $\mathbf{X}(k)$ and $\mathbf{Q}$ is the variance matrix of $\mathbf{W}(k)$.

Step 4. Extended Kalman filtering iteration.

4.1 Set the priors: $\mathbf{X}^{-}(k)=\mathbf{X}(k-1)$; $\mathbf{P}^{-}(k)=\mathbf{P}(k-1)+\mathbf{Q}$

4.2 Update the filter: $\mathbf{K}(k)=\mathbf{P}^{-}(k)\mathbf{H}^{T}(k)\left(\mathbf{H}(k)\mathbf{P}^{-}(k)\mathbf{H}^{T}(k)+\mathbf{R}\right)^{-1}$

4.3 Estimate the posts: $\mathbf{X}(k)=\mathbf{X}^{-}(k)+\mathbf{K}(k)\left[\mathbf{z}(k)-h\left(\mathbf{X}^{-}(k)\right)\right]$

4.4 Update the $\mathbf{P}$ matrix: $\mathbf{P}(k)=\left[\mathbf{I}-\mathbf{K}(k)\mathbf{H}(k)\right]\mathbf{P}^{-}(k)$

Step 5. Go back to Step 1 for next interval.

NUMERICAL EXAMPLE

Experimental Design

To assess the proposed models' potential for field applications, this study used an arterial segment of Guangming 6th Road in Chupei, Taiwan, for a case study. The geometric layout of the target arterial and its topology are shown in Figure 5. The arterial consists of five intersections, 12 nodes, and 34 links. Also, both Intersections 3 and 4 contain one freeway on-ramp and one off-ramp. Hence, the number of O-D flows to be estimated is reduced to 48 per time interval.

To replicate the field traffic conditions, this study used Vissim as the simulation platform and used the observed intersection queues and

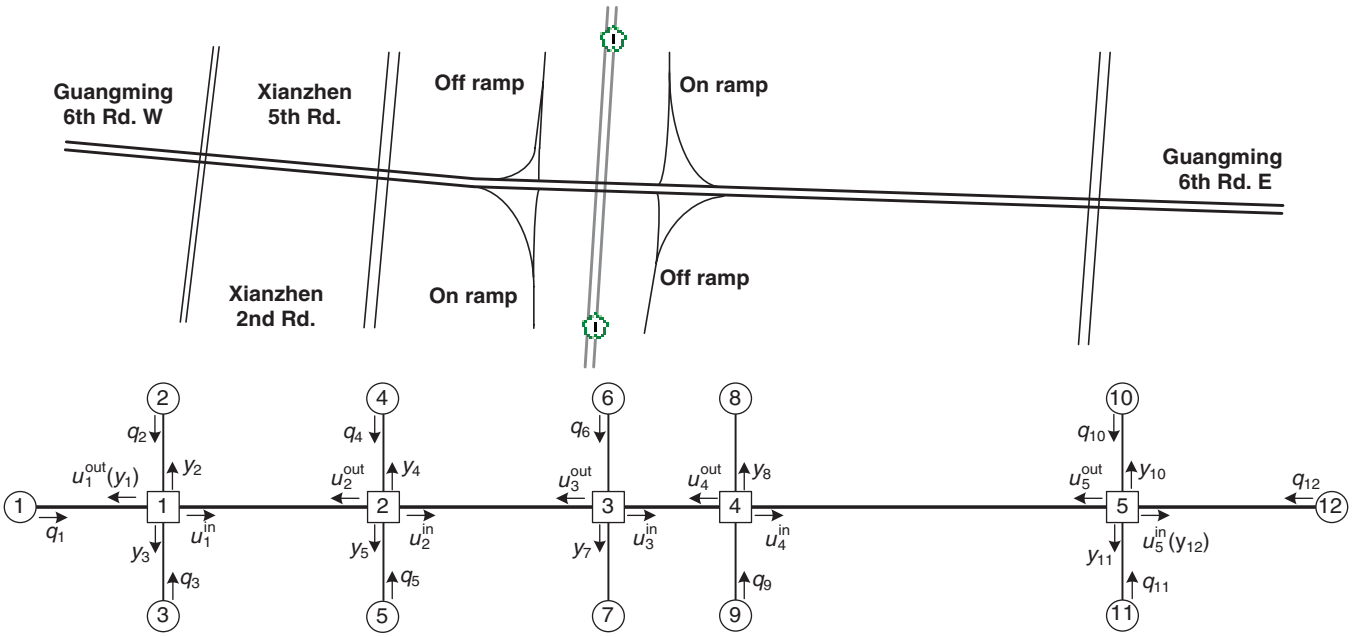

FIGURE 5 Geometric layout of study site.

link volumes from 16:30 to 21:30 on April 24, 2013, for calibration. Because a simulated system is meaningful only if it can faithfully reflect actual traffic patterns, this study performed the calibration by minimizing the differences between simulated and field-collected queues and turning flow rates at intersections. The calibrated simulation was then used to generate simulated scenarios for model evaluation. Table 1 summarizes the demand patterns from each source generated with the simulated system, in which the simulation period is 2 h and four time periods (30 min each). The phasing plan, signal timings, and original phase sequence at each intersection are presented in Figure 6. The common cycle length was 150 s.

Using the well-calibrated Vissim network, the study took advantage of the following information for model assessment: (*a*) GPS data with a 1-s time interval for each vehicle and (*b*) loop detector and queue detector data. Then, one can use GPS data to track the trajectory of each vehicle and subsequently identify the ground-truth O-D flow patterns. The three proposed models required different sets of detectors. For Model 1, each link upstream was installed with one loop detector for flow data collection; and loop detectors were installed downstream of each link in Model 2 to capture the turning flows at each intersection. For Model 3, four additional queue detectors were needed at those four links between neighboring intersections (i.e., Intersections 2 and 3 and Intersections 4 and 5).

Model Evaluation and Results

To evaluate the effectiveness of the proposed three models, the dynamic O-D flows estimated with the different models were compared with the ground-truth O-D flows obtained with GPS data. Model 1 was treated as a benchmark for measuring the benefits of the other two enhanced models. Comparisons of estimation accuracy were based on three key outputs: link flow counts, turning flows at all intersections, and dynamic O-D flows.

The quality of accuracy is measured with the following indicators: mean absolute error (MAE), mean absolute percentage error (MAPE), and root mean square error (RMSE). All performance indicators are defined as follows:

$$\mathrm{MAE} = \frac{1}{N}\sum_{i=1}^{N}\left|x_i - \hat{x}_i\right|$$

TABLE 1 Time-Varying Entry Flows from Each Source Node

Time Period (s)	Node Number									
	1	2	3	4	5	6	9	10	11	12
0–1,800	560	210	210	753	547	882	1,470	420	490	840
1,800–3,600	640	240	240	860	625	1,008	1,680	480	560	960
3,600–5,400	720	270	270	968	703	1,134	1,890	540	630	1,080
5,400–7,200	640	240	240	860	625	1,008	1,680	480	560	960

NOTE: Demand unit: vehicles per hour.

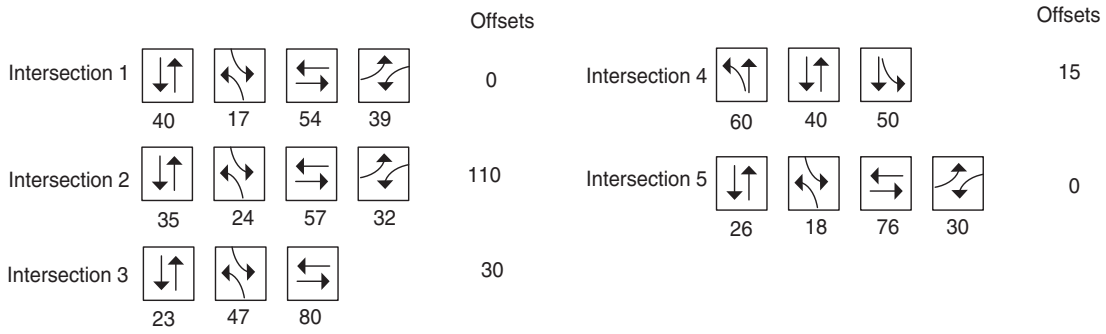

FIGURE 6 Signal timings and initial phase sequences.

$$\text{MAPE} = \frac{1}{N}\sum_{i=1}^{N}\left|\frac{x_i - \hat{x}_i}{\hat{x}_i}\right|$$

$$\text{RMSE} = \sqrt{\frac{1}{N}\sum_{i=1}^{N}(x_i - \hat{x}_i)^2}$$

where x_i and $\hat{x}_i$ are the estimated and the ground-truth values, and N is the number of estimated states.

Table 2 summarizes all the performance indicators for O-D flows, link flows, and turning flows given by the models. According to the results, Model 1 can produce an accurate estimate of link flows, and its resulting MAPE is about 15.86%. Link flows are the major measurements in Model 1, and the estimation results are corrected with a Kalman filter over subsequent time intervals. However, Model 1 cannot yield a sufficiently reliable estimate for both turning flows and O-D flows, as shown in Table 2, where the errors can reach as high as 42% in MAPE. The target arterial with Model 1 has 28 available measurements for estimation but has more than 300 unknown parameters.

With turning flows at each intersection as the measurements, Model 2 outperforms Model 1 in estimating O-D patterns. As shown in Table 2, the MAPE of turning flows and O-D flows with Model 2 have been reduced to 18.27% and 33.20%, respectively. The sum of turning flows at each link equals the collected link flows when travel time impact is neglected. However, a comparison of the results between the two models shows that increasing the number of observable measurements can improve estimation accuracy.

As shown by the results in Table 2, Model 3 can produce the most accurate estimates compared with the other two models. The estimated accuracy with respect to link flows, turning flows, and O-D flows, based on MAPE, is 15.92%, 17.46%, and 28.11%, respectively. Model 3 takes real-time queue information at several critical links as the additional measurement over Model 2. Comparing the results of Model 2 and Model 3 confirms the effectiveness of incorporating the queue information. For instance, according to the data in Table 2, the improvements for O-D flow estimation by Model 3 compared with Model 2 with respect to MAE, MAPE, and RMSE are calculated as 15.07%, 15.33% and 21.21%, respectively.

Identification of Critical Path Flows by Using Estimated O-D Patterns

A reliable estimate of arterial O-D flows offers essential information for identifying the critical traffic paths (O-D pairs) for design of signal progression. Therefore, the critical paths identified with the three O-D models are compared next. Those critical paths were identified by ranking the O-D volumes and eliminating those pairs spanning only one intersection.

As shown in Table 3, both Model 1 and Model 2 can identify only three of six actual critical paths. However, Model 3 can identify all six critical paths with the correct rankings. Therefore, one could argue that the enhanced model is more reliable for identifying major path-flow patterns in the design of a multipath signal progression system. Verifying the effectiveness of incorporating real-time queue information in O-D flow estimation, Figure 7 compares estimated and actual O-D flows.

As shown in Figure 7, *a* and *b*, all three models can capture the pattern of the first two critical O-D flows (7→10 and 6→10), and produce acceptable estimates. Figure 7, *c* and *d*, indicates that both Model 1 and Model 2 do not yield sufficiently reliable estimates for two key O-D flows (7→1 and 6→4). In contrast, Model 3 can still capture the flow patterns from these two O-D paths. Further investigation of such estimation discrepancies shows that both Node 1 and

TABLE 2 Estimation Accuracy of O-D Flows

	Model 1			Model 2			Model 3		
Flow	MAE	MAPE (%)	RMSE	MAE	MAPE (%)	RMSE	MAE	MAPE (%)	RMSE
Link	4.54	18.56	5.48	4.10	16.31	5.21	3.99	15.92	4.99
Turning	4.02	42.39	5.54	2.75	18.27	4.07	2.70	17.46	3.92
O-D	1.885	42.02	3.075	1.473	33.20	2.512	1.251	28.11	1.979

NOTE: The unit of MAE and RMSE is vehicle.

TABLE 3 Ground Truth and Identified Critical Paths from Proposed Models

Ground Truth		Basic Model 1		Basic Model 2		Enhanced Model	
O-D Pair	Total Flows	O-D Pair	Total Flows	O-D Pair	Total Flows	O-D Pair	Total Flows
9→12	1,390	9→12	1,658	9→12	1,372	9→12	1,480
6→12	765	6→12	985	6→12	860	6→12	784
9→1	756	9→4	649	9→4	727	9→1	722
6→4	729	4→7	497	4→7	571	6→4	642
12→7	553	4→8	465	12→8	544	12→7	540
12→1	472	9→1	427	9→1	531	12→1	452

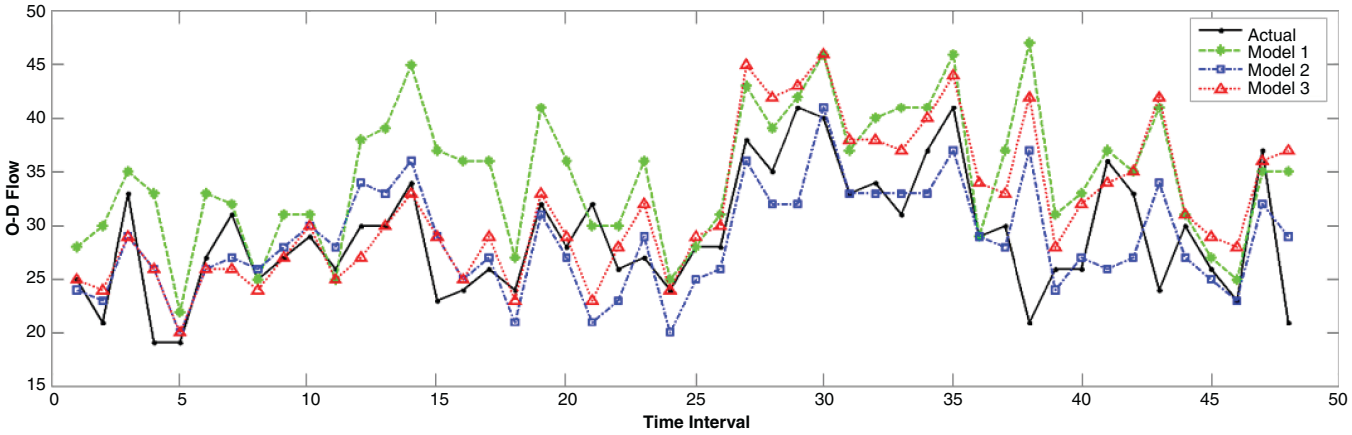

(a)

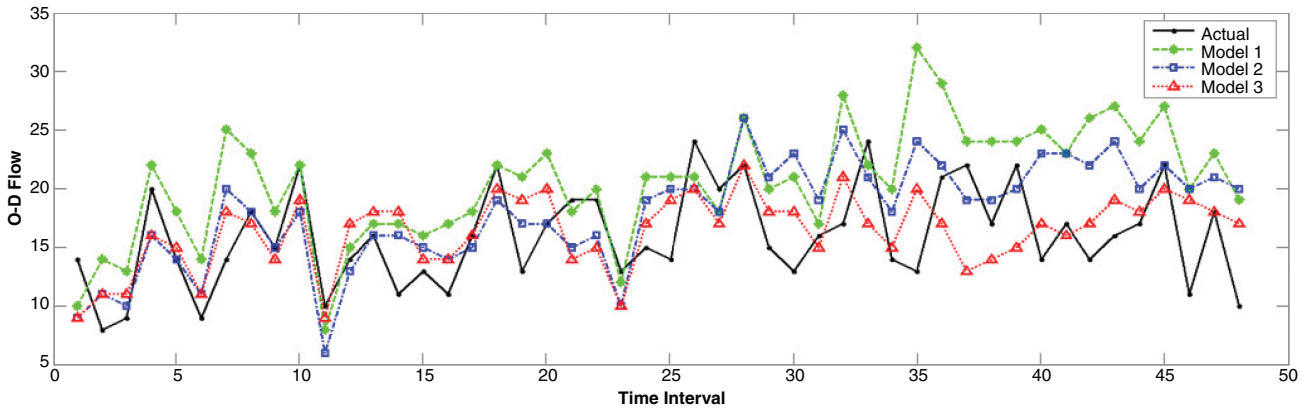

(b)

FIGURE 7 Time-dependent flows for critical O-D pairs: (*a*) 7 → 10 and (*b*) 6 → 10.
(continued)

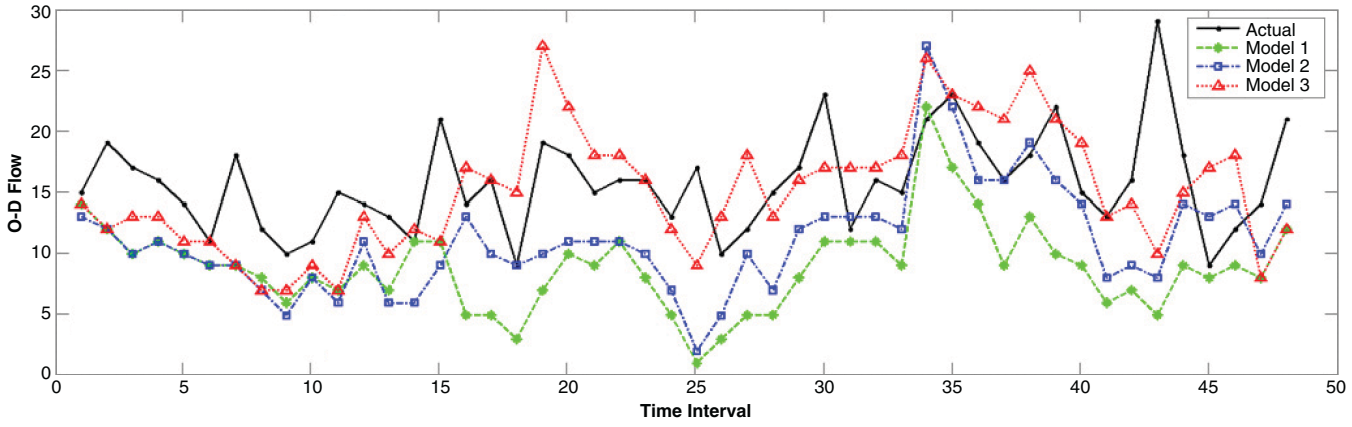

(c)

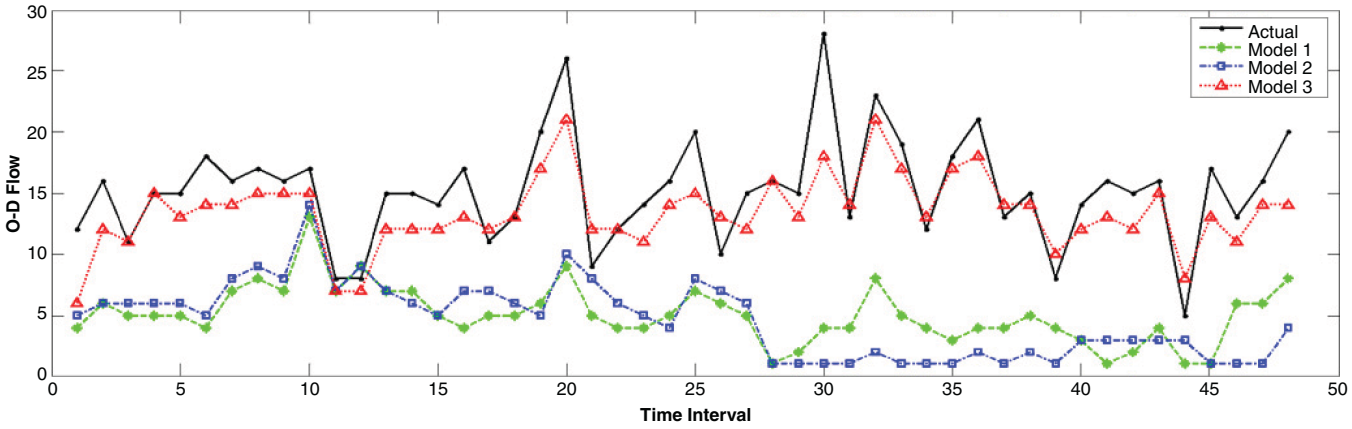

(d)

FIGURE 7 *(continued)* Time-dependent flows for critical O-D pairs: (*c*) 7 → 1 and (*d*) 6 → 4.

Node 4 have high exiting flows. Also, there are two major source flows (from Node 6 and Node 9) that may contribute to those exit flows. In the ground-truth flow patterns, most exit flows via Node 4 are from the source node, Node 6. However, both Models 1 and 2 fail to capture such relationships and underestimate the O-D flows (7→1) but overestimate the O-D flows (6→4). Since the existing signal plan at this study site was designed to coordinate the through traffic from Intersection 3 to Intersection 1, the high O-D flows (6→4) and (7→1) caused a long right-turn queue but a relatively short through queue. Hence, taking real-time queue information as the additional measurements in Model 3 can produce a much more reliable estimate.

CONCLUSIONS

This paper presented three models for estimating the dynamic O-D flows on a signalized arterial. Model 1 uses link counts as the main measurements, whereas Model 2 directly takes intersection turning flows as its primary input. Recognizing the impacts of O-D patterns and signal plans on the intersection queue distribution, Model 3 further incorporates the real-time queue patterns as additional measurements to improve the estimation accuracy. All three models can be solved with a sequential algorithm based on the extended Kalman filter.

On the basis of the actual arterial flows and O-D information, the study conducted extensive numerical experiments to assess the performance of these proposed models, especially with respect to their ability to identify critical arterial path flows, based on their respective volumes. The comparison results show that Model 3, which incorporates time-varying intersection queue information, can yield the best estimation accuracy and can correctly identify and rank all critical path flows according to their respective volumes. Such promising results offer valuable information traffic engineers can use to design a multipath signal progression system, rather than the conventional through-flow-based progression (*1*).

Although increasing the number of queue detectors on arterial links would increase the number of measurements and could consequently improve estimation accuracy, it also would require much higher installation and maintained costs. Hence, extensions of this study will focus on advancing the proposed models to select the most critical links that need queue detectors, whereas estimation accuracy could still be guaranteed.

ACKNOWLEDGMENTS

The authors are grateful for the data provided by the National Chiao Tung University and for its project sponsored by Taiwan Ministry of Communications and Transportation. This study was partially

supported by a National Science Foundation grant and by an Infrastructure Management in Extreme Events project, Integrated Stage-Based Evacuation with Social Perception Analysis and Dynamic Population Estimation.

REFERENCES

1. Yang, X., Y. Cheng, and G.L. Chang. A Multi-Path Progression Model for Synchronization of Arterial Traffic Signals. *Transportation Research Part C: Emerging Technologies,* Vol. 53, 2015, pp. 93–111. https://doi.org/10.1016/j.trc.2015.02.010.
2. Lou, Y., and Y. Yin. A Decomposition Scheme for Estimating Dynamic Origin–Destination Flows on Actuation-Controlled Signalized Arterials. *Transportation Research Part C: Emerging Technologies,* Vol. 18, No. 5, 2010, pp. 643–655. https://doi.org/10.1016/j.trc.2009.06.005.
3. Chang, G.L., and X. Tao. Estimation of Time-Dependent Turning Fractions at Signalized Intersections. *Transportation Research Record: Journal of the Transportation Research Board,* No. 1644, 1998, pp. 142–149. https://doi.org/10.3141/1644-15.
4. Zockaie, A., Y. Chen, and H.S. Mahmassani. Adaptive Drivers and Time-Dependent Origin–Destination Demand Estimation: Methodology and Application to Large-Scale Network. Presented at 93rd Annual Meeting of the Transportation Research Board, Washington, D.C., 2014.
5. Verbas, İ.O., H.S. Mahmassani, and K. Zhang. Time-Dependent Origin–Destination Demand Estimation: Challenges and Methods for Large-Scale Networks with Multiple Vehicle Classes. *Transportation Research Record: Journal of the Transportation Research Board,* No. 2263, 2011, pp. 45–56. https://doi.org/10.3141/2263-06.
6. Nie, Y., and H.M. Zhang. A One-Level O-D Estimation Approach Based on Relaxation. Presented at 86th Annual Meeting of the Transportation Research Board, Washington, D.C., 2007.
7. Cascetta, E. Estimation of Trip Matrices from Traffic Counts and Survey Data: A Generalized Least Squares Estimator. *Transportation Research Part B: Methodological,* Vol. 18, No. 4–5, 1984, pp. 289–299. https://doi.org/10.1016/0191-2615(84)90012-2.
8. Sherali, H.D., and T. Park. Estimation of Dynamic Origin–Destination Trip Tables for a General Network. *Transportation Research Part B: Methodological,* Vol. 35, No. 3, 2001, pp. 217–235. https://doi.org/10.1016/S0191-2615(99)00048-X.
9. Lu, C.C., X. Zhou, and K. Zhang. Dynamic Origin–Destination Demand Flow Estimation Under Congested Traffic Conditions. *Transportation Research Part C: Emerging Technologies,* Vol. 34, 2013, pp. 16–37. https://doi.org/10.1016/j.trc.2013.05.006.
10. Bell, M.G. The Real Time Estimation of Origin–Destination Flows in the Presence of Platoon Dispersion. *Transportation Research Part B: Methodological,* Vol. 25, No. 2–3, 1991, pp. 115–125. https://doi.org/10.1016/0191-2615(91)90018-E.
11. Chang, G.-L., and J. Wu. Recursive Estimation of Time-Varying Origin–Destination Flows from Traffic Counts in Freeway Corridors. *Transportation Research Part B: Methodological,* Vol. 28, No. 2, 1994, pp. 141–160. https://doi.org/10.1016/0191-2615(94)90022-1.
12. Chang, G.-L., and X. Tao. Estimation of Dynamic O-Ds for Urban Networks. *Transportation and Traffic Flow Theory,* Vol. 13, 1996, pp. 1–20.
13. Chang, G.-L., and X. Tao. An Integrated Model for Estimating Time-Varying Network Origin–Destination Distributions. *Transportation Research Part A: Policy and Practice,* Vol. 33, No. 5, 1999, pp. 381–399. https://doi.org/10.1016/S0965-8564(98)00038-X.
14. Zhou, X., and H.S. Mahmassani. Dynamic Origin–Destination Demand Estimation Using Automatic Vehicle Identification Data. *IEEE Transactions on Intelligent Transportation Systems,* Vol. 7, No. 1, 2006, pp. 105–114. https://doi.org/10.1109/TITS.2006.869629.
15. Castillo, E., J.M. Menéndez, and P. Jiménez. Trip Matrix and Path Flow Reconstruction and Estimation Based on Plate Scanning and Link Observations. *Transportation Research Part B: Methodological,* Vol. 42, No. 5, 2008, pp. 455–481. https://doi.org/10.1016/j.trb.2007.09.004.
16. Parry, K., and M.L. Hazelton. Estimation of Origin–Destination Matrices from Link Counts and Sporadic Routing Data. *Transportation Research Part B: Methodological,* Vol. 46, No. 1, 2012, pp. 175–188. https://doi.org/10.1016/j.trb.2011.09.009.
17. Cao, P., T. Miwa, T. Yamamoto, and T. Morikawa. Bilevel Generalized Least Squares Estimation of Dynamic Origin–Destination Matrix for Urban Network with Probe Vehicle Data. *Transportation Research Record: Journal of the Transportation Research Board,* No. 2333, 2013, pp. 66–73. https://doi.org/10.3141/2333-08.
18. Iqbal, M.S., C.F. Choudhury, P. Wang, and M.C. González. Development of Origin–Destination Matrices Using Mobile Phone Call Data. *Transportation Research Part C: Emerging Technologies,* Vol. 40, 2014, pp. 63–74. https://doi.org/10.1016/j.trc.2014.01.002.
19. Su, D., R. Horowitz, and X.-Y. Lu. Real-Time Estimation of Intersection Turning Proportions from Exit Counts. Presented at 93rd Annual Meeting of the Transportation Research Board, Washington, D.C., 2014.
20. Lee, S., S.C. Wong, C.C.C. Pang, and K. Choi. Real-Time Estimation of Lane-to-Lane Turning Flows at Isolated Signalized Junctions. *IEEE Transactions on Intelligent Transportation Systems,* Vol. 16, No. 3, 2015, pp. 1549–1558. https://doi.org/10.1109/TITS.2014.2365876.
21. *Highway Capacity Manual 2010.* Transportation Research Board of the National Academies, Washington, D.C., 2010.

The Standing Committee on Transportation Network Modeling peer-reviewed this paper.